American Mineralogist, Volume 104, pages 1638–1649, 2019

Al and Si diffusion in rutile

Daniele J. Cherniak[1,*] and E. Bruce Watson[1]

[1]Department of Earth and Environmental Sciences, Rensselaer Polytechnic Institute, Troy, New York 12180, U.S.A.

Abstract

Diffusion of Al and Si has been measured in synthetic and natural rutile under anhydrous conditions. Experiments used Al_2O_3 or Al_2O_3-TiO_2 powder mixtures for Al diffusant sources, and SiO_2-TiO_2 powder mixtures or quartz-rutile diffusion couples for Si. Experiments were run in air in crimped Pt capsules, or in sealed silica glass ampoules with solid buffers (to buffer at NNO or IW). Al profiles were measured with Nuclear Reaction Analysis (NRA) using the reaction $^{27}Al(p,\gamma)^{28}Si$. Rutherford Backscattering spectrometry (RBS) was used to measure Si diffusion profiles, with RBS also used in measurements of Al to complement NRA profiles. We determine the following Arrhenius relations from these measurements: For Al diffusion parallel to *c*, for experiments buffered at NNO, over the temperature range 1100–1400 °C:

$$D_{Al} = 1.21 \times 10^{-2} \exp(-531 \pm 27 \text{ kJ/mol}^{-1}/RT) \text{ m}^2\text{s}^{-1}.$$

For Si diffusion parallel to c, for both unbuffered and NNO-buffered experiments, over the temperature range 1100–1450 °C:

$$D_{Si} = 8.53 \times 10^{-13} \exp(-254 \pm 31 \text{ kJ/mol}^{-1}/RT) \text{ m}^2\text{s}^{-1}.$$

Diffusion normal to (100) is similar to diffusion normal to (001) for both Al and Si, indicating little diffusional anisotropy for these elements. Diffusivities measured for synthetic and natural rutile are in good agreement, indicating that these diffusion parameters can be applied in evaluating diffusivities in rutile in natural systems Diffusivities of Al and Si for experiments buffered at IW are faster (by a half to three-quarters of a log unit) than those buffered at NNO.

Si and Al are among the slowest-diffusing species in rutile measured thus far. Diffusivities of Al and Si are significantly slower than the diffusion of Pb and slower than the diffusion of tetravalent Zr and Hf and pentavalent Nb and Ta. These data indicate that Al compositional information will be strongly retained in rutile, providing evidence for the robustness of the recently developed Al in rutile thermobarometer. For example, at 900 °C, Al compositional information would be preserved over ~3 Gyr in the center of 250 μm radius rutile grains, but Zr compositional information would be preserved for only about 300 000 yr at this temperature. Al-in-rutile compositions will also be much better preserved during subsolidus thermal events subsequent to crystallization than those for Ti-in-quartz and Zr-in-titanite crystallization thermometers.

Keywords: Rutile, diffusion, aluminum, silicon, Rutherford backscattering, nuclear reaction analysis, geothermometry, geobarometry

Introduction

Rutile, found in various geological settings, can incorporate significant amounts of trivalent, divalent, and pentavalent cations, including several high field strength elements, with concentrations up to tens of percentages (e.g., Vlassopoulos et al. 1993). The geochemical behavior of these trace and minor elements in rutile can offer insight into the subduction zone processes (e.g., Ryerson and Watson 1987; Brenan et al. 1994; Stalder et al. 1998; Foley et al. 2000; Zack et al. 2002; Ewing and Müntener 2018); HFSE with multiple valence states incorporated in rutile also have the potential to provide information on f_{O_2} conditions (e.g., Liu et al. 2014; Guo et al. 2017). Since rutile tends to remain stable during sedimentary and diagenetic processes, its trace element signatures can reveal information about provenance (e.g., Morton and Hallsworth 1999; Zack et al. 2002), and may be used in geospeedometry (e.g., Kohn et al. 2016; Cruz-Uribe et al. 2018). The Zr-in-rutile geothermobarometer (Degeling 2003; Zack et al. 2004b; Watson et al. 2006; Tomkins et al. 2007) has been increasingly applied in a range of studies to assess crystallization temperatures and/or pressures (e.g., Ewing et al. 2013; Taylor-Jones and Powell 2015; Pape et al. 2016; Mitchell and Harley 2017; Tual et al. 2018). Rutile is also used as a U-Pb geochronometer (e.g., Corfu and Andrews

* E-mail: chernd@rpi.edu

0003-004X/19/0011–1638$05.00/DOI: https://doi.org/10.2138/am-2019-7030

1986; Corfu and Muir 1989; Mezger et al. 1989, 1991; Schandl et al. 1990; Wong et al. 1991; Davis 1997; Smye and Stockli 2014).

In this work, we report results for Si and Al diffusion in natural and synthetic rutile, with evaluation of the effects of oxygen fugacity and crystallographic orientation on diffusion. These data supplement and complement earlier measurements of diffusion of trace and minor elements in rutile and may permit a greater general understanding of diffusion-controlled processes in rutile.

Most notably, recent experimental work (Hoff and Watson 2018) has shown the potential for use of Al concentrations in rutile as a geothermobarometer. Al concentrations in rutile may also affect diffusion of other species, such as Cr (e.g., Sasaki et al. 1985). Taylor-Jones and Powell (2015) have proposed that slow-diffusing Si in rutile may lead to the slowing of Zr diffusion, resulting in higher retentivity of Zr and higher closure temperatures. However, Kohn et al. (2016) have argued against the hypothesis of Zr coupling with slower-diffusing Si, asserting instead that high Zr contents (and thus high Zr-in-rutile temperatures) observed in UHT rocks are a consequence of the degree to which the surfaces of rutile crystals are able to maintain equilibrium with matrix minerals, including zircon and baddeleyite. Despite possible complexities in natural systems, measurements of Si diffusion in rutile are of value given the ubiquity of silicon in geologic systems, as well as the utility of these diffusivities in understanding processes such as the exsolution of zircon needles in rutile (e.g., Pape et al. 2016).

Slightly reduced and doped rutiles, as semiconducting materials, have been used in a range of technological applications. Al-doped rutile has been developed as an optical material (e.g., Hatta et al. 1996); Si can also be added to rutile to tailor optical properties (Gonzalez-Elipe et al. 2006; Demiryont 1985). Al is a common additive to TiO_2 pigments to enhance photochemical stability and may have large effects on the conductivity of rutile and its polymorphs (Bak et al. 2003) and on crystal growth and transformation kinetics (Gesenhues 1997; Gesenhues and Rentschler 1999; Karvinen 2003). Understanding the diffusion of key dopant species in rutile can assist in refining production processes and provide constraints on the long-term integrity of these materials.

Experimental procedure and materials

The majority of diffusion experiments in this study were run on synthetic rutile. The synthetic rutile, from the MTI Corporation, was purchased in the form of wafers polished on one side, in either (001) or (100) orientation. To explore the effects of the presence of trace and minor elements on diffusion, some Si diffusion experiments were run using a natural rutile. The natural rutile, from Pennsylvania, was from the same specimen as used in our earlier studies of Pb, Hf, and Zr diffusion in rutile (Cherniak et al. 2007a; Cherniak 2000). Minor and trace element concentrations from LA-ICP-MS analyses of the rutile (based on averages of 3 or 6 point analyses on synthetic and natural rutile grains, respectively) are presented in Table 1. The wafers of synthetic rutile were cut into square pieces, about 2 mm on a side. The natural rutile was cut normal to c into slabs about 0.5 mm thick, polished with SiC papers and alumina powders down to 0.3 μm, and finished with a chemical polish using colloidal silica.

Si diffusion experiments were conducted using quartz-rutile diffusion couples or with powder sources containing SiO_2. The powder sources used were either dried SiO_2 powder, or a mixture of TiO_2 and SiO_2 powders in 3:1 (by wt.) ratio, ground under ethanol, dried, and heated in a Pt crucible for one day at 1250 °C. The SiO_2-TiO_2 powder sources worked well for experiments run in air, but the buffered experiments run in sealed silica glass capsules showed significant Si-rich material clinging to rutile sample surfaces following diffusion anneals, which precluded successful analysis of these samples. As a consequence, only quartz-rutile diffusion couples were used in buffered experiments.

Table 1. Trace and minor element compositions of rutile from LA-ICP-MS analyses

Element (ppm)	Natural rutile (PA)	Synthetic rutile
Al	330 ± 25	26 ± 9
V	1326 ± 32	–
Cr	538 ± 24	–
Fe	3063 ± 220	8 ± 4
Ni	279 ± 26	–
Zr	113 ± 6	–
Nb	2738 ± 101	–
Hf	5.9 ± 0.3	–
Ta	119 ± 3	–
W	65 ± 3	–

For the Al diffusion experiments, sources of diffusant were Al_2O_3 powder, or mixtures of TiO_2 and Al_2O_3 powders, in either 3:1 or 10:1 (by wt.) ratios. The TiO_2-Al_2O_3 powder mixtures were ground under ethanol, dried, and heated in Pt crucibles for one day at 1250 °C. To explore the potential effects of coupled substitutions on Al diffusion, an experiment was run that incorporated Nb into the source material. For this source, the TiO_2-Al_2O_3 10:1 wt. ratio powder mixture was combined with Nb_2O_5 powder in a weight ratio of 100:1.

For powder-source experiments, rutile crystals were surrounded by the source powders in Pt capsules, and capsules crimped shut. Diffusion couples were created by placing polished faces of rutile and synthetic quartz slabs in contact, tying the couple together with Pt wire, and wrapping the couple in Pt mesh. For experiments run under buffered conditions, the Pt capsules or diffusion couples were placed inside a silica glass ampoule with another crimped Pt capsule containing the buffer material (mixtures of Ni metal and nickel oxide powders to buffer at NNO, or FeO powder and Fe flakes to buffer at IW); silica glass chips were used to physically separate the samples and buffer capsules inside the silica glass ampoule. The sample-buffer assemblies were then sealed in the silica ampoule under vacuum.

All experiments were run in one-atmosphere tube furnaces with $MoSi_2$ heating elements, with sample temperatures monitored by type S (Pt-Pt10%Rh) thermocouples with temperature uncertainties of ~±2 °C. Experiments were then removed from the furnace and allowed to cool in air. The rutile crystals were extracted from capsules and cleaned ultrasonically in distilled H_2O and ethyl alcohol. Experimental conditions and durations for Si and Al diffusion experiments are presented in Tables 2 and 3.

Time-series studies were performed for both Al and Si diffusion to establish that the measured concentration profiles are due to volume diffusion and are not a result of other processes such as surface reaction that could lead to enhanced concentrations of the diffusant in the near-surface region. For these time series, a set of Si diffusion experiments was performed at 1300 °C for experiments ranging from 19 h to one week in duration, and a set of Al diffusion experiments at 1250 °C for 1 to 6 days.

Nuclear Reaction Analysis (NRA) of Al

The Al diffusion experiments were analyzed using nuclear reaction analysis (NRA) with the reaction $^{27}Al(p,\gamma)^{28}Si$. These analyses were performed at the Ion Beam Laboratory at the University at Albany, using proton beams produced by the Dyamitron accelerator. For Al profiling, the 992 keV resonance of the reaction was employed, with a bismuth germanate (BGO) detector used to detect γ rays produced in the reaction (Cherniak 1995; Cherniak and Watson 1992; Tailby et al. 2018). Energy steps of 1.0–0.5 keV for the incident proton beam were taken near the resonance energy to profile Al at depths near the sample surface, with larger energy steps (2–5 keV) at greater depths (above ~150 nm). Spectra from untreated specimens of rutile were also recorded at each energy step to evaluate background levels in the γ energy region of interest, and γ spectra of Al foil were collected as a standard to convert γ yields into Al concentrations for rutile samples. Typical detection limit for analytical conditions used in this work is ~100 ppm atomic. Depth scales for the Al profiles were calculated from the energy difference between the incident proton beam and the resonance energy, and by the stopping power (energy loss of the

protons as a function of depth in the material); stopping powers used in-depth calculations were determined with the software SRIM (Ziegler and Biersack 2006).

RBS analysis

Si diffusion experiments were analyzed with RBS. In addition, Al diffusion experiments were measured with RBS to complement the NRA analyses described above. RBS has been used as the primary analytical method in many of our diffusion studies, including measurements of Pb, Zr, and Hf diffusion in rutile (Cherniak 2000; Cherniak et al. 2007a). The analytical procedures used here are similar, with a $^4He^+$ incident beam of 2 or 3 MeV energy used for analysis. RBS spectra were converted to Si and Al concentration profiles using procedures similar to those described in other work (e.g., Cherniak 1993). Si (and Al) signals rest on those from He backscattered from Ti in the sample, resulting in high backgrounds, so detection limits are on order of a few tenths of an atomic percent, but Si concentrations are relatively high in the samples (up to a few at%, at the highest temperatures of the experiments), so peaks can be well-resolved from background signals. For Al, in cases where both RBS and NRA measurements of samples were made (as discussed below), diffusivities agreed within experimental uncertainties.

TABLE 2. Al diffusion in rutile

	T (°C)	Time (s)	*D* (m^2s^{-1})	log*D*	B	buffer	C_o[b]	Source[a]
			normal to (001)					
RuAl-11	1100	1.72×10^6	3.78×10^{-23}	−22.42	0.41	NNO	0.69	10:1
RuAl-7	1151	9.43×10^5	3.93×10^{-22}	−21.41	0.17	NNO	3.91	3:1
RuAl-10	1150	7.83×10^5	3.84×10^{-22}	−21.42	0.34	NNO	0.73	10:1
RuAl-24	1150	3.51×10^5	1.99×10^{-21}	−20.70	0.16	IW	3.81	10:1
RuAl-1	1200	4.28×10^5	1.64×10^{-21}	−20.78	0.18	UB	6.89	3:1
RuAl-2	1200	2.59×10^5	2.26×10^{-21}	−20.65	0.16	NNO	5.71	3:1
RuAl-9	1200	4.18×10^5	1.76×10^{-21}	−20.75	0.25	NNO	1.05	10:1
RuAl-20	1200	2.59×10^5	1.30×10^{-21}	−20.89	0.17	NNO	5.64	10:1+Nb
RuAl-3	1250	1.67×10^5	7.38×10^{-21}	−20.13	0.15	NNO	7.65	3:1
RuAl-16	1250	8.64×10^4	1.02×10^{-20}	−19.99	0.14	NNO	3.81	10:1
RuAl-12	1250	1.66×10^5	8.01×10^{-21}	−20.10	0.11	NNO	4.60	10:1
RuAl-15	1250	5.45×10^5	6.48×10^{-21}	−20.19	0.13	NNO	1.42	10:1
RuAl-19	1250	2.02×10^5	9.33×10^{-21}	−20.03	0.10	UB	2.02	Al_2O_3
RuAl-23	1250	5.45×10^5	2.03×10^{-20}	−19.69	0.08	IW	5.16	10:1
RuAl-4	1300	6.84×10^4	2.89×10^{-20}	−19.54	0.13	NNO	9.97	3:1
RuAl-13	1300	9.24×10^4	2.87×10^{-20}	−19.54	0.12	NNO	3.70	10:1
RuAl-6	1350	5.04×10^4	7.12×10^{-20}	−19.15	0.16	NNO	7.65	3:1
RuAl-14	1350	5.40×10^4	6.18×10^{-20}	−19.21	0.12	NNO	4.05	10:1
RuAl-22	1350	6.12×10^4	2.22×10^{-19}	−18.65	0.08	IW	7.13	10:1
RuAl-5	1400	1.80×10^4	5.50×10^{-19}	−18.26	0.26	NNO	4.50	3:1
			(100)					
RuAl-17	1200	3.35×10^5	2.14×10^{-21}	−20.67	0.16	NNO	1.07	10:1
RuAl-18	1300	7.56×10^4	4.89×10^{-20}	−19.31	0.23	NNO	1.14	10:1

[a] 3:1–3:1 ratio (by wt.) TiO_2:Al_2O_3; 10:1–10:1 ratio (by wt.) TiO_2:Al_2O_3.
[b] Surface concentration in at%.

Fitting of depth profiles

RBS and NRA depth profiles were fit with a model to determine the diffusion coefficient (*D*). Diffusion is modeled as simple one-dimensional, concentration-independent diffusion in a semi-infinite medium with a source reservoir maintained at constant concentration (i.e., a complementary error function solution). The rationale for the use of this model has been discussed in previous publications (e.g., Cherniak and Watson 1992). Diffusivities are evaluated by plotting the inverse of the error function (i.e., $\text{erf}^{-1}\{[C_o - C(x,t)]/C_o\}$) vs. depth ($x$) in the sample. A straight line of slope $(4Dt)^{-1/2}$ results if the data conform to a complementary error function solution. C_o, the surface concentration of diffusant, is independently determined by iteratively varying its value until the intercept of the line con-

TABLE 3. Si diffusion in rutile

	T (°C)	Time (s)	*D* (m^2s^{-1})	log*D*	±	Buffer	C_o[a]	Source
				normal to (001)				
RuSi-38	1100	9.49×10^5	2.02×10^{-22}	−21.69	0.40	NNO	0.63	diff couple
RuSi-11	1149	9.50×10^5	5.50×10^{-22}	−21.26	0.34	UB	1.89	TiO_2:SiO_2
RuSi-34	1151	5.11×10^5	6.76×10^{-22}	−21.17	0.39	NNO	0.99	diff couple
RuSi-42	1150	3.51×10^5	2.92×10^{-21}	−20.53	0.17	IW	3.81	diff couple
RuSi-1	1200	3.53×10^5	6.39×10^{-22}	−21.19	0.35	UB	1.09	SiO_2
RuSi-31	1200	2.82×10^5	1.56×10^{-21}	−20.81	0.34	UB	0.69	diff couple
RuSi-32	1200	2.48×10^5	1.52×10^{-21}	−20.82	0.23	NNO	1.73	diff couple
RuSi-2	1250	1.98×10^5	1.30×10^{-21}	−20.88	0.20	UB	1.74	SiO_2
RuSi-37	1250	2.45×10^5	9.36×10^{-22}	−21.03	0.21	NNO	4.15	diff couple
RuSi-41	1250	2.56×10^5	1.31×10^{-20}	−19.88	0.20	IW	2.99	diff couple
RuSi-3	1301	7.56×10^4	3.36×10^{-21}	−20.47	0.20	UB	1.66	SiO_2
RuSi-4	1301	6.84×10^4	3.97×10^{-21}	−20.40	0.31	UB	1.15	TiO_2:SiO_2
RuSi-20	1299	5.83×10^5	2.15×10^{-21}	−20.67	0.18	UB	3.46	TiO_2:SiO_2
RuSi-21	1299	2.54×10^5	2.43×10^{-21}	−20.61	0.18	UB	3.34	TiO_2:SiO_2
RuSi-28	1300	8.64×10^4	8.85×10^{-21}	−20.05	0.29	UB	0.94	SiO_2
RuSi-35	1300	8.64×10^4	2.30×10^{-21}	−20.64	0.44	NNO	2.19	diff couple
RuSi-7	1351	5.76×10^4	8.23×10^{-21}	−20.08	0.18	UB	4.12	TiO_2:SiO_2
RuSi-36	1350	7.56×10^4	3.79×10^{-21}	−20.42	0.14	NNO	7.17	diff couple
RuSi-40	1350	7.56×10^4	4.41×10^{-20}	−19.36	0.27	IW	1.40	diff couple
RuSi-6	1400	1.44×10^4	1.19×10^{-20}	−19.92	0.20	UB	4.88	TiO_2:SiO_2
RuSi-39	1400	1.44×10^4	1.78×10^{-20}	−19.75	0.29	NNO	4.98	diff couple
RuSi-8	1450	7.20×10^3	2.22×10^{-20}	−19.65	0.19	UB	8.96	TiO_2:SiO_2
				normal to (100)				
RuSi-10	1200	3.46×10^5	4.80×10^{-22}	−21.32	0.29	UB	0.77	TiO_2:SiO_2
RuSi-13	1299	9.00×10^4	5.00×10^{-21}	−20.30	0.30	UB	0.64	TiO_2:SiO_2
RuSi-19	1399	5.94×10^4	1.22×10^{-20}	−19.91	0.28	UB	1.19	TiO_2:SiO_2
				natural rutile, cut parallel to c				
NRuSi-9	1150	4.28×10^5	3.26×10^{-22}	−21.49	0.46	NNO	0.95	diff couple
NRuSi-8	1250	6.48×10^4	3.02×10^{-21}	−20.52	0.38	NNO	0.96	diff couple
NRuSi-10	1350	1.62×10^4	1.35×10^{-20}	−19.87	0.18	NNO	4.78	diff couple

[a] Surface concentration in at% percent.

verges on zero. In Figure 1, typical diffusion profiles for both Al and Si are shown. The uncertainties in concentration and depth from each data point (mainly derived from counting statistics and backgrounds in the former and RBS detector resolution in the latter) were used to evaluate the uncertainties in the diffusivities determined from the fits to the model.

Results

The results for Al diffusion are plotted in Figure 2 and presented in Table 2. Diffusivities obtained with NRA and RBS agree within uncertainties. There is little evidence of diffusional anisotropy. Al diffusion appears to have a weak negative dependence on oxygen fugacity, with diffusivities under IW-buffered conditions about half a log unit higher than those under NNO-buffered conditions. Samples run with the 3:1 TiO_2:Al_2O_3 source generally have higher surface concentrations than samples run with the 10:1 source (typically 2–6× higher at a given temperature under NNO-buffered conditions), but diffusivities agree within experimental uncertainty. Surface concentrations of the diffusant also display a broad trend of increasing with increasing temperature. For diffusion normal to (001), for experiments buffered at NNO, we obtain an activation energy of 531 ± 27 kJ/mol and pre-exponential factor of 1.21 × 10^{-2} m^2s^{-1} (logD_o = –1.92 ± 0.92).

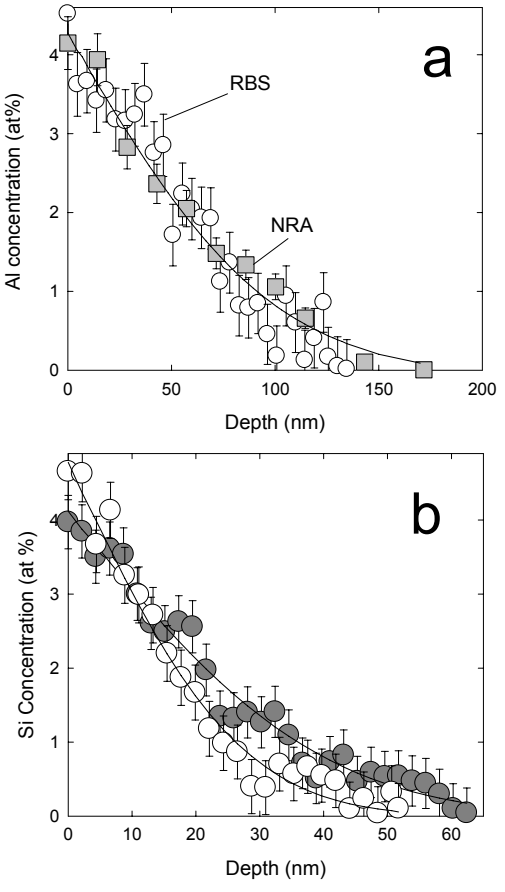

Figure 1. Example Al (**a**) and Si (**b**) diffusion profiles for rutile. The Al experiment [on synthetic rutile, with diffusion normal to (001)] was run at 1400 °C for 5 h. Profiles from both RBS and NRA, using the $^{27}Al(p,\gamma)^{28}Si$ reaction, are plotted. The Si profiles are from an experiment on synthetic rutile run at 1350 °C for 16 h (gray symbols), and for an experiment on natural rutile run for 4.5 h at 1350 °C (white symbols).

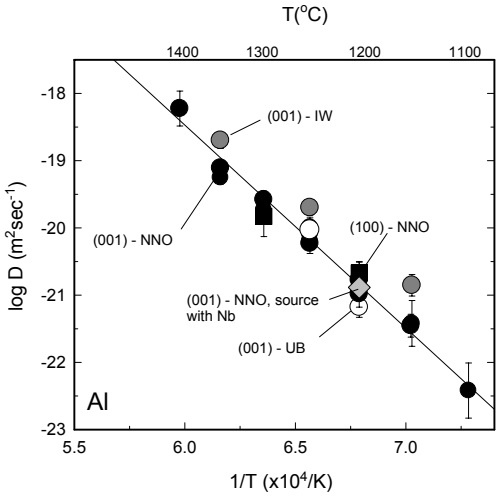

Figure 2. Arrhenius plot of Al diffusion data for rutile. For diffusion normal to (001), for experiments buffered at NNO, we obtain an activation energy of 531 ± 27 kJ/mol and pre-exponential factor of 1.21 × 10^{-2} m^2s^{-1} (logD_o = –1.92 ± 0.92). There appears to be little anisotropy when comparing diffusion normal to (001) and (100). Diffusion under IW-buffered conditions is faster by about half a log unit.

A time series at 1250 °C, conducted for Al diffusion in rutile normal to (001), with experiments run for times ranging from 24 h to more than 6 days (Fig. 3a), results in diffusivities that are con-

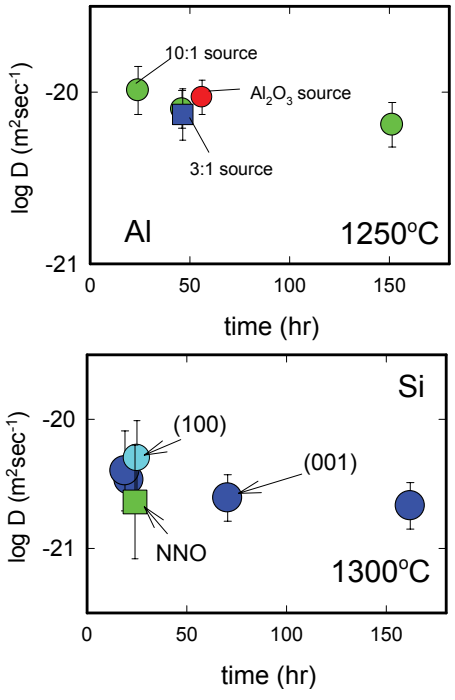

Figure 3. Time series for Al (**a**) and Si (**b**) at 1250 and 1300 °C, respectively. For both elements, diffusivities are quite similar over times varying by more than a factor of 6, suggesting that volume diffusion is the dominant contributor to the observed diffusion profiles. (Color online.)

sistent within experimental uncertainty, providing evidence that volume diffusion, rather than other phenomena such as surface reaction, is the dominant contributor to the measured diffusion profiles over this range of conditions. No anomalously shaped profiles are observed for Al (or Si) that would be suggestive of concentration-dependence of diffusion, and experiments with sources containing different concentrations of diffusant yield diffusivities that agree within experimental uncertainty.

Diffusion data for Si are plotted in Figure 4 and presented in Table 3. For Si diffusion perpendicular to (001) in synthetic rutile under unbuffered conditions, we obtain an activation energy of 275 ± 45 kJ/mol and a pre-exponential factor 4.41×10^{-12} m^2s^{-1} ($\log D_o = -11.36 \pm 1.38$). There is little evidence of diffusional anisotropy when comparing diffusivities normal to (100) and (001). For diffusion under NNO-buffered conditions in synthetic rutile, normal to (001), an activation energy of 216 ± 48 kJ/mol and a pre-exponential factor 4.07×10^{-14} m^2s^{-1} ($\log D_o = -13.39 \pm 1.62$) are obtained. A fit to both the NNO-buffered and unbuffered data results in an activation energy of 254 ± 31 kJ/mol and a pre-exponential factor 8.53×10^{-13} m^2s^{-1} ($\log D_o = -12.07 \pm 1.03$). Diffusivities of Si in natural rutile under NNO-buffered conditions do not differ significantly from those obtained for NNO-buffered synthetic rutile, indicating that differences in trace and minor element compositions between the synthetic and natural materials have little effect on diffusion, a finding consistent with observations for Hf and Pb diffusion (Cherniak 2000; Cherniak et al. 2007a). Like Al, Si diffusion exhibits a negative dependence on oxygen fugacity when comparing diffusivities under NNO- and IW-buffered conditions.

As with Al, a time series for Si diffusion in rutile normal to (001) was run, in this case at 1300 °C for times ranging from 19 h to a week (Fig. 3b). Diffusivities are in agreement within experimental uncertainties, suggesting that volume diffusion is the dominant contributor to the observed Si diffusion profiles.

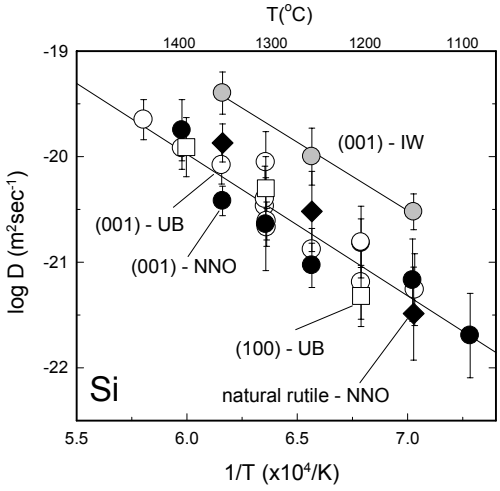

FIGURE 4. Arrhenius plot of Si diffusion data for synthetic and natural rutile. For Si diffusion perpendicular to (001) in synthetic rutile under unbuffered conditions, we obtain an activation energy of 275 ± 45 kJ/mol and a pre-exponential factor 4.41×10^{-12} m^2s^{-1} ($\log D_o = -11.36 \pm 1.38$). There is little evidence of diffusional anisotropy when comparing diffusivities normal to (100) and (001). For diffusion under NNO-buffered conditions in synthetic rutile, normal to (001), an activation energy of 216 ± 48 kJ/mol and a pre-exponential factor 4.07×10^{-14} m^2s^{-1} ($\log D_o = -13.39 \pm 1.62$) are obtained; a fit to both the NNO-buffered and unbuffered data results in an activation energy of 254 ± 31 kJ/mol and a pre-exponential factor 8.53×10^{-13} m^2s^{-1} ($\log D_o = -12.07 \pm 1.03$). Diffusivities of Si in natural rutile under NNO-buffered conditions do not differ significantly from those obtained for NNO-buffered synthetic rutile, indicating that differences in trace and minor element compositions between the synthetic and natural materials have little effect on diffusion. Like Al, Si diffusion exhibits a negative dependence on oxygen fugacity; diffusivities under IW-buffered conditions are about three quarters of a log unit faster than under NNO-buffered conditions.

Comparison with diffusivities of other elements in rutile and potential diffusion mechanisms

A summary of selected diffusion data for cations in rutile is plotted in Figure 5. Si and Al are among the slowest-diffusing species in rutile measured to date. Si diffuses about 6 orders of magnitude slower than Ti. Diffusivities of Al and Si are significantly lower than those of divalent cations, including the large divalent cations Pb and Ba (Nakayama and Sasaki 1963; Cherniak 2000) and other trivalent cations, including Sc and Cr (Sasaki et al. 1985). Al and Si also diffuse more slowly than tetravalent Zr and Hf and pentavalent Nb and Ta (Cherniak et al. 2007a; Marschall et al. 2013; Dohmen et al. 2018). For example, Si diffusion is about 2 orders of magnitude slower than the Zr diffusivities determined by Cherniak et al. (2007a), and about 3 orders of magnitude slower than Pb diffusion; Al diffusion is about 6 orders of magnitude slower than Nb diffusion, and 9 orders of magnitude slower than Cr diffusion (Sasaki et al. 1985).

Trivalent and more highly charged cations, which may migrate via a coupled interstitial/interstitialcy mechanism (Zhu et al. 2017), and divalent cations of large ionic radius such as Ba (Nakayama and Sasaki 1963) and Pb (Cherniak 2000), do not show pronounced diffusional anisotropy. This contrasts with the significant diffusional anisotropy of small divalent cations, which travel interstitially through open channels in the rutile structure along the c-axis (Sasaki et al. 1985), a mechanism consistent with findings from DFT calculations (Zhu et al. 2017).

Al^{3+} predominately substitutes for Ti^{4+} on normal octahedral sites at lower pressures, but higher pressures induce the incorporation of Al^{3+} into octahedral interstices of the rutile structure (Escudero et al. 2012). Al solubility increases with increasing temperature (Stebbins 2007) and pressure, with 10 wt% Al_2O_3 in rutile at 1300 °C and 7 GPa (Escudero et al. 2012), with concentrations at 1 atm in the range of 1–2 wt% Al_2O_3 (Slepetys and Vaughan 1969; Escudero et al. 2012); these values are broadly consistent with surface concentrations determined for the lower-temperature experiments using the 10:1 TiO_2:Al_2O_3 source. For samples with up to 1 wt% Al_2O_3, Al is found in ordered, isolated octahedral (Ti sites), while at higher concentrations, Al predominates in disordered octahedral sites, with possible contributions from both Ti sites with Al neighbors and interstitials (Stebbins 2007). The substitution of Al in Ti sites may be compensated for by oxygen vacancies (Hatta et al. 1996; Islam et al. 2007); while interstitial substitutions are possible, substitution on Ti lattice sites is energetically favorable. The larger size of Al compared with Si, along with the potential for migrating via defect complexes to preserve local charge balance, may lead to the higher activation energy for diffusion observed for Al.

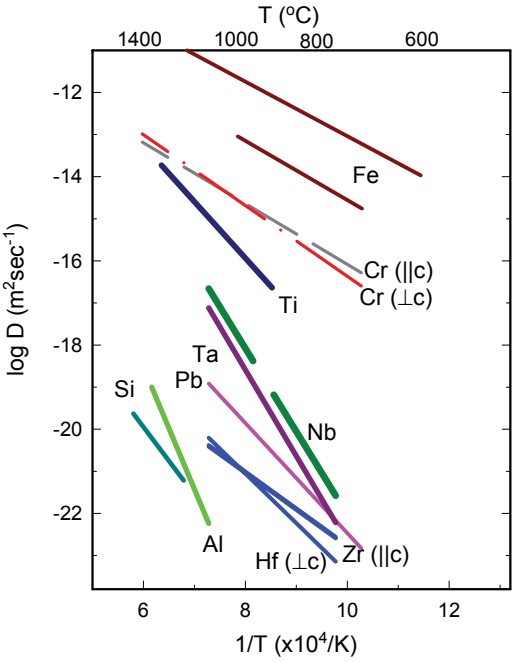

FIGURE 5. Selected cation diffusion data for rutile. Sources for data: Cr, Fe = Sasaki et al. (1985); Ti-Akse and Whitehurst 1978; Nb, Ta = Marschall et al. (2013); Hf, Zr = Cherniak et al. (2007a); Pb = Cherniak (2000); Al, Si = this study. (Color online.)

In contrast, because of its small size compared with Ti, Si may have an off-center position in the rutile lattice, and may also occupy interstitial positions (Golden et al. 2015), which could contribute to the lower activation energy for Si diffusion. As with Al, Si solubilities in rutile increase with increasing temperature and pressure (Ren et al. 2009), with solubilities, for example, of ~1.5 wt% at 10 GPa and 1800 °C, and ~5 wt% at 2000 °C and 23 GPa. While it is difficult to extrapolate down to lower pressure and temperature conditions, about half of our Si surface concentrations fall below the former value.

The influence of point defect chemistry on chemical diffusion in rutile is discussed in numerous publications (e.g., Nowotny et al. 2006a, 2006b; 2012). The principal atomic defects in undoped rutile are titanium interstitials and oxygen and titanium vacancies (e.g., Marucco et al. 1981; Hoshino et al. 1985; Bak et al. 2012). There are two kinetic regimes associated with the diffusion-controlled equilibration kinetics of TiO_2. The first is controlled by transport of rapidly moving defects (oxygen vacancies, titanium interstitials) and the second is determined by the transport of titanium vacancies that diffuse much more slowly; this results in a difference in diffusivities between the two regimes of about 4 orders of magnitude (Nowotny et al. 2006a, 2006b).

Additional point defects will be present if altervalent impurities reside on Ti sites in rutile. Common substitutional impurities in natural rutile are the pentavalent cations Nb and Ta, ferric and ferrous iron, as well as other transition elements and Al (Deer et al. 1992). Electrostatic balance for pentavalent cations is commonly achieved by vacancies in cation sites, or by complementary substitution of divalent or trivalent cations (such as Fe) on Ti lattice sites. The pentavalent cations Ta and Nb diffuse much more rapidly than Al (Marschall et al. 2013; Dohmen et al. 2018) and our results indicate that the presence of pentavalent cations as potential charge compensating species appears to have little effect on Al diffusion. For divalent and trivalent cations, charge compensation may be via oxygen vacancies or Ti interstitials. Experimental and theoretical studies suggest that trivalent species such as Cr and Sc, and tetravalent Zr are likely to diffuse via an interstitialcy mechanism that involves tetravalent interstitial Ti ions (Sasaki et al. 1985; Zhu et al. 2017). The diffusion rates for these cations (along with Ti self-diffusion; e.g., Akse and Whitehurst 1978) have a dependency on oxygen fugacity to the negative one-fifth power [$D \sim (pO_2)^{-1/5}$], which provides supporting evidence for tetravalent Ti interstitials as the controlling point defect. Recent work by Dohmen et al. (2018) on diffusion of tetravalent (Zr, Hf) and pentavalent (Nb, Ta) cations in rutile has determined the presence of two different diffusion mechanisms: (1) an interstitialcy mechanism involving trivalent Ti on interstitial sites, and (2) a vacancy mechanism involving Ti vacancies. The former is dominant at lower f_{O_2} (<QFM+2 log units), as well as at high temperatures (above 1350 °C), and has a negative dependence on f_{O_2}, with the latter the dominant mechanism at higher f_{O_2} (>QFM+2) and having diffusivities largely independent of f_{O_2}.

Both Si and Al diffusivities appear broadly consistent with a negative dependence on f_{O_2}, suggesting an interstitialcy mechanism. In contrast to Al, activation energies for diffusion of Si are similar to those for Ti. While we do not have full understanding of lattice diffusion mechanisms from the results of this study, the data reported are from experiments conducted under conditions of geologic relevance. These results indicate that Al and Si diffusion are not greatly affected by the differing amounts of minor and trace elements present in the synthetic and natural rutiles. However, it is important to note that while Al and Si concentrations in these experiments approach those that could be found in mantle-derived rutile, they are much higher than concentrations generally found in crustal rutile, which range up to several hundred parts per million (e.g., Zack et al. 2004a). The present data, given the detection limits for analysis and the relatively high concentrations of Al and Si in diffusion experiments, do not preclude the occurrence of differing diffusion mechanisms at lower concentrations of Al and Si.

The effects of pressure and water or other hydrous species on diffusion rates are also considerations in applying these experimental results. Pressure effects on diffusion in rutile have not been extensively explored, but they are unlikely to be large for geologically reasonable pressure ranges. There has been some investigation of the effects of hydrous species on oxygen diffusion (Moore et al. 1998), which indicates that oxygen diffusion in rutile grown in the presence of water, or in rutile grains reduced in such an environment, is about an order of magnitude slower than in rutile reduced under anhydrous conditions, but there is little evidence to date of the influence of hydrous species on cation diffusion.

Although the potential effects of the factors of concentration and the presence of hydrous species on Al and Si diffusion are not fully resolved, we apply our diffusion data (with the caveats above) in simple calculations and comparisons in the sections that follow.

Si and Al diffusion in other minerals compared with rutile

A summary of data for Al and Si diffusion is plotted in Figure 6. As in rutile, Al diffusion in Al_2O_3 has a high activation energy for diffusion, and diffusivities are comparable in magnitude to those for rutile. Al diffusion is much faster in MgO, olivine, quartz, and magnetite. Si diffusion in rutile is slower than quartz, MgO, and labradorite, but faster than Si in zircon, anorthite, and olivine, and comparable to silicate perovskite and diopside over the temperature range under which experiments were conducted. However, given the differences in activation energies for diffusion, Si diffusion in rutile will be faster than in most other minerals at lower temperatures (below ~1000 °C) with the exception of diopside and MgO.

Béjina and Jaoul (1997) found that diffusion parameters obtained for Si diffusion in silicates conform to a linear compensation law when the activation energy for diffusion is plotted as a function of the log of the pre-exponential factor. This compensation relation, using the data tabulated in Béjina and Jaoul (1997), a few more recent results, including that for zircon from Cherniak (2008), was described in Cherniak (2008) by the equation $E = 647.7 + 30.5 \cdot \log D_o$. Béjina and Jaoul (1997) argue that compensation behavior may be explained by the "strain energy" model proposed in Zener (1952) in which the Gibbs free energy of diffusion is considered the "elastic work" required to place the defect in its excited state for migration within the lattice. They note that differences in activation enthalpies among individual materials are likely due to differences in the coupling of point defects that minimize the migration energy for Si through the lattice, and/or the characteristic "extrinsicity" of the material (based on its impurity levels, non-stoichiometry, presence of aliovalent cations, and other factors).

Interestingly, our diffusion parameters for Si in rutile fall closely along the compensation trend (Fig. 7). If we interpret our findings in light of these observations, the relatively low activation energy for Si diffusion in rutile may be in part attributable to the greater possibility of non-stoichiometry of rutile and the potential for the coupling of point defects in ways that may reduce the energies for Si migration through the mineral lattice (e.g., Béjina and Jaoul 1997). Diffusion parameters for Si in MgO (Sakaguchi et al. 1992) also fall along the compensation trend. Whether this conformity to a diffusion compensation trend for Si diffusion applies to other non-silicates remains unclear, but these results may be suggestive of a more generalized applicability of the Meyer-Neldel Rule (diffusion compensation law) for Si diffusion. As Jones (2014) has noted, when considering the case of a single diffusing species in a range of mineral phases, it may be the case that those minerals with a large average activation barrier (high E_a) compensate with increased frequency of attempts to diffuse (larger D_o) (e.g., Boisvert et al. 1995), thus resulting in these diffusion compensation trends.

Diffusion in mineral–element pairs used as geothermobarometers

Figure 8 presents a summary of data for diffusion of mineral-element pairs employed in crystallization geothermo(baro)meters. These mineral-element pairs include Zr-in-rutile (Degeling 2003; Zack et al. 2004b; Watson et al. 2006; Ferry and Watson 2007; Tomkins et al. 2007), Ti-in-zircon (Watson and Harrison 2005; Watson et al. 2006; Ferry and Watson 2007), Ti-in-quartz (Wark and Watson 2006; Thomas et al. 2010), and Zr-in-titanite (Hayden et al. 2008), and Al-in-rutile (Hoff and Watson 2018). The Al diffusion data from the present work and measurements of diffusivities for the other mineral-element pairs (Cherniak 2006; Cherniak and Watson 2007; Cherniak et al. 2007a, 2007b) can be used to evaluate the relative resistance of these geothermometers to diffusional alteration when these mineral phases experience subsolidus thermal events following crystallization. For comparison, we also plot our data for Si diffusion.

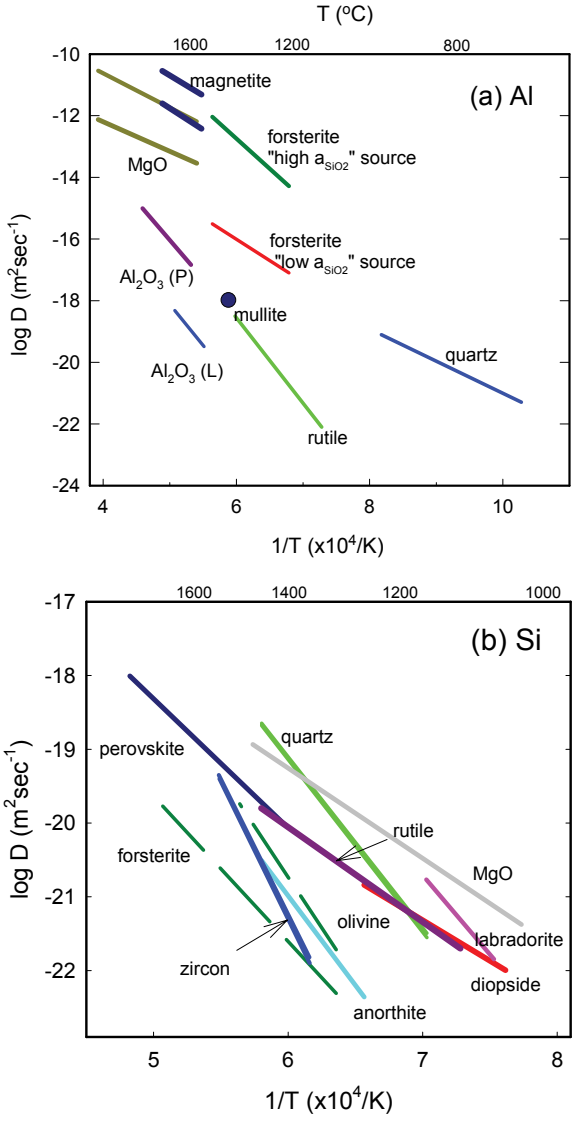

Figure 6. (**a**) Al diffusion data for selected minerals. Sources for data: quartz = Tailby et al. 2018; forsterite = Zhukova et al. 2017; MgO = Van Orman et al. 2009; Al_2O_3 = LeGall et al. 1994; Paladino and Kingery 1962; magnetite = Dieckmann et al. 1978; mullite = Fielitz et al. 2006. (**b**) Si diffusion data for selected minerals. Sources for data: quartz, anorthite, labradorite = Cherniak 2003; zircon = Cherniak 2008; forsterite = Jaoul et al. 1981; olivine = Dohmen et al. 2002; MgO = Sakaguchi et al. 1992; diopside = Béjina and Jaoul 1996; perovskite = Yamazaki et al. 2000. (Color online.)

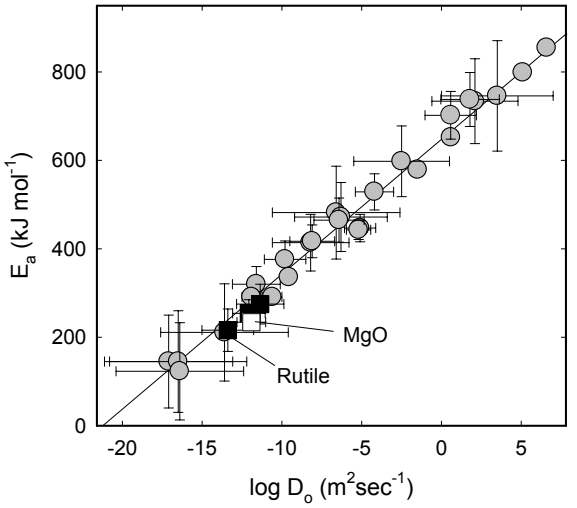

FIGURE 7. Plot of activation energy (in kJ/mol) vs. the log of the pre-exponential factor D_o, showing that Si diffusion data for silicates conform well to the linear "diffusion compensation" relation outlined by Béjina and Jaoul (1997) and Cherniak (2008). The compensation line can be described by the equation $E = 647.7 + 30.5\log D_o$. Data plotted are from Béjina and Jaoul (1997) and Cherniak (2008). Results for Si diffusion in rutile from the present study (dark squares) are also plotted. These fall closely along the diffusion compensation trend, as does that for Si diffusion in MgO (white square).

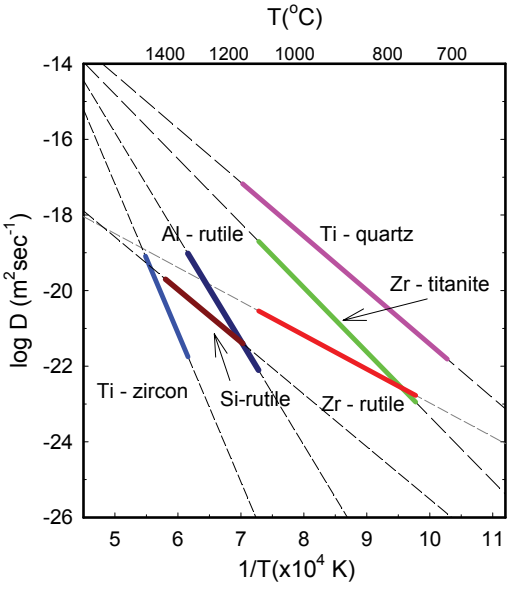

FIGURE 8. Summary of data for diffusion of mineral-element pairs employed in selected crystallization geothermometers. Sources for data: Ti–zircon: Cherniak and Watson (2007); Zr–rutile: Cherniak et al. (2007a); Zr–titanite; Cherniak (2006); Ti–quartz: Cherniak et al. (2007b); Al–rutile: this study. (Color online.)

Diffusion of Al-in-rutile is faster than Ti diffusion in zircon but considerably slower than Ti diffusion in quartz, and slower than Zr diffusion in titanite and rutile under geologically relevant conditions. For example, at 800 °C, Al diffusion in rutile would be about 5 orders of magnitude faster than Ti diffusion in zircon, but 7 orders of magnitude slower than Ti diffusion in quartz, and ~5 and 6 orders of magnitude slower than Zr diffusion in rutile and titanite, respectively.

At 800 °C, Si would diffuse more slowly than Zr in rutile by about 2 orders of magnitude. Although slower diffusivities of Si with respect to Zr-in-rutile are unlikely to influence temperatures derived from Zr-in-rutile thermometry (Kohn et al. 2016), Si diffusion may be rate-limiting for other processes, such as the exsolution of zircon needles in rutile. Also, Si is a significant trace component of natural rutile whose concentration has been shown to be particularly sensitive to pressure (Gaetani et al. 2008; Ren et al. 2009; Mosenfelder et al. 2010; Escudero and Langenhorst 2012). Based in part on the data of Gaetani et al. (2008), Taylor-Jones and Powell (2015) proposed a preliminary equation to describe the T and P dependence of Si uptake in rutile in equilibrium with quartz and zircon. A comprehensive experimental calibration may emerge in the foreseeable future, which would elevate the importance of our new diffusion law for Si to a new level. Taylor-Jones and Powell (2015) emphasized the potential value of a high closure temperature (T_C) for Si diffusion in rutile, contrasting with the relatively low T_C value for Zr diffusion (see next section).

The relatively low diffusivity of Al indicates that the Al-in-rutile geothermobarometer (Hoff and Watson 2018) will be resistant to diffusional resetting under a broad range of geologic conditions. In the following section, we will evaluate time-temperature scenarios under which these records may be preserved or compromised.

Preservation of chemical signatures for various crystallization thermometers

Using the diffusion data reported in this work, we can illustrate how well specific crystallization geothermometers may preserve past temperatures with calculations that constrain conditions under which resetting of Al, Si, Zr, or Ti chemical signatures (and therefore information about crystallization temperatures) may take place. For a simple example, we use a model in which the mineral grains are spheres of radii a having an initial uniform concentration of diffusant C_1, which are exposed to an external medium with diffusant concentration C_o. Based on these initial and boundary conditions, a solution to the diffusion equation at the center of the spheres can be derived (e.g., Crank 1975). For circumstances when the dimensionless parameter Dt/a^2 (where D is the diffusion coefficient and t is the time) has a value less than or equal to 0.03, the concentration at the center of the sphere will remain unchanged from the initial value. This can be referred to as a "center retention" criterion. At greater values of Dt/a^2, concentrations of diffusant at the sphere's center will be is affected by the external concentration C_o. If we consider an infinite cylinder geometry (better suited for many rutile grains), a similar model can be applied with a as the radius of the cylinder; for this model, the relevant value of the center-retention parameter Dt/a^2 is ~0.04.

In Figure 9, sets of curves for Dt/a^2 for the values of these dimensionless parameters are plotted, using effective diffusion radii that represent typical grain sizes for each mineral. These

values of radii *a* are 0.5 mm for quartz, 250 μm for rutile and titanite, and 50 μm for zircon. The curves define the time-temperature limits under which initial Al, Si, Zr, or Ti compositional information will be preserved in the grain centers of each mineral, with concentrations at crystal cores remaining unaltered for conditions below the curves, but affected by the surrounding medium for conditions above the curves. These plots demonstrate that crystallization conditions estimated from Al concentrations in rutile will be far more resistant to diffusional alteration than those from the Zr-in-rutile thermometer. For example, at 900 °C, Al compositional information would be preserved over ~3 Gyr in the center of 250 μm radius rutile grains, but Zr compositional information would be preserved for only about 300 000 yr at this temperature. Al-in-rutile compositions will also be much better preserved during subsolidus thermal events subsequent to crystallization than those for Ti-in-quartz and Zr-in-titanite crystallization thermometers. In general, the likelihood of preservation of Si concentrations in rutile falls between that for Zr and Al.

The conclusions summarized above can be graphically illustrated in a manner that simulates X-ray maps that could be obtained on individual rutile crystals in natural rocks. Concentration contour maps are well-suited to portraying the spatial distribution (and therefore diffusion progress) of elements in natural crystals, as a complement to the sometimes intuitively elusive dimensionless quantity Dt/a^2. To this end, we ran simulations of Si, Al, and Zr diffusion in rutile crystals with the goal of contouring the resulting concentrations in 2D section to illustrate and compare results. In this case, our model crystal was a cylindrical rutile grain 200 μm in diameter and 600 μm long; calculations were performed using the CYLMOD computer program written by Watson et al. (2010) for the purpose of modeling diffusion in finite cylinders. The concentration of the elements was held constant at the cylinder surface at an arbitrary value below the initial (uniform) concentration within the cylinder. The broad objective was to illustrate outcomes for the three elements that span behaviors from nearly closed (very limited diffusion) to badly compromised. An isothermal heating event lasting 10 million years was used for this comparison; results are shown in Figure 10 as concentration contours within the rutile cylinder expressed in terms of percent of the initial uniform value. For the time span considered, diffusion progress for Al, Si, and Zr is approximately the same (and very limited) at 900, 700, and 500 °C, respectively. The three diffusants also show similar progress (66–78% overall retention) at 950, 800, and 600 °C, respectively. Higher temperatures result pronounced open-system behavior, as shown by the bottom row of panels in Figure 10.

All of the preceding discussion applies to isothermal conditions. Given the availability of diffusion laws for the relevant elements, the possibility of open-system behavior during both prograde and retrograde metamorphism can also be readily addressed. Resetting of thermobarometers during geologic cooling can be evaluated qualitatively using the well-known closure-temperature equation of Dodson (1973), which returns closure temperatures for Al, Si, and Zr in rutile of ~1050, ~930, and ~700 °C for spherical grains of 250 μm radius cooling at 10 °C/Myr. Similarly, there may be instances where rutile

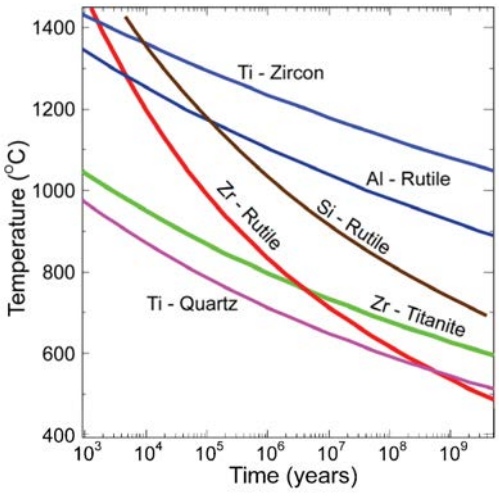

FIGURE 9. Curves representing time-temperature conditions for mineral-element pairs used in crystallization thermometers under which Ti, Zr, Al, or Si signatures at the center of grains will be lost. For times and temperatures below the curves, concentrations at crystal cores will remain unaffected, but they will be influenced by the surrounding medium when conditions above the curves apply. In calculations, diffusivities from the Arrhenius relations plotted in Figure 8 are used, and effective diffusion radii differing with mineral type are selected to reflect grain sizes typical for each mineral: 50 μm for zircon, 0.5 mm for quartz, and 250 μm for both rutile and titanite. Rutile will be considerably more retentive of Al compositions at grain centers than Zr; for example, at 900 °C, Zr signatures would be altered in times of ~300 000 yr, while Al signatures would be preserved at this temperature over times on order 3 billion years. (Color online.)

crystallizes in a metabasite at relatively low temperature and is subsequently heated with increasing metamorphic grade, possibly resetting one or more thermobarometers. In this case, it is instructive to explore both center retention (defined as above), and diffusive "opening," which we define as a 1% diffusive loss or gain of the element of interest—i.e., incipient open-system behavior. Diffusive "opening" and center retention during linear heating of spherical grains are readily evaluated using the generalized expression of Watson and Cherniak (2013):

$$T_{\mathrm{rt}\%} = \frac{0.457 \cdot (E_\mathrm{a} / \mathrm{R})}{\chi_\mathrm{h} + \log\left[\dfrac{E_\mathrm{a} \cdot D_0}{\mathrm{R} \cdot dT / dt \cdot a^2}\right]} \quad (1)$$

where D_o and E_a are the Arrhenius parameters for the diffusant of interest, dT/dt is the heating rate, a is the radius of the grain domain, R is the gas constant, and χ_h is a constant describing the fraction of change in the amount. For a given heating trajectory, $T_{\mathrm{rt}\%}$ is the temperature (in kelvins) at which a specific fractional retention (or loss) is reached, and where the constant χ_h will have a specific value depending on the amount of fractional loss. For retention levels of 50% and 99%, the center retention and diffusive opening criteria defined above, χ_h has values of –0.785 and 2.756, respectively. In calculations, we use a linear heating rate of 10 °C/Myr and plot opening and center retention temperatures for Al as a function of grain radius in Figure 11. For comparison, we also plot conditions for diffusive opening of both Zr and Pb in

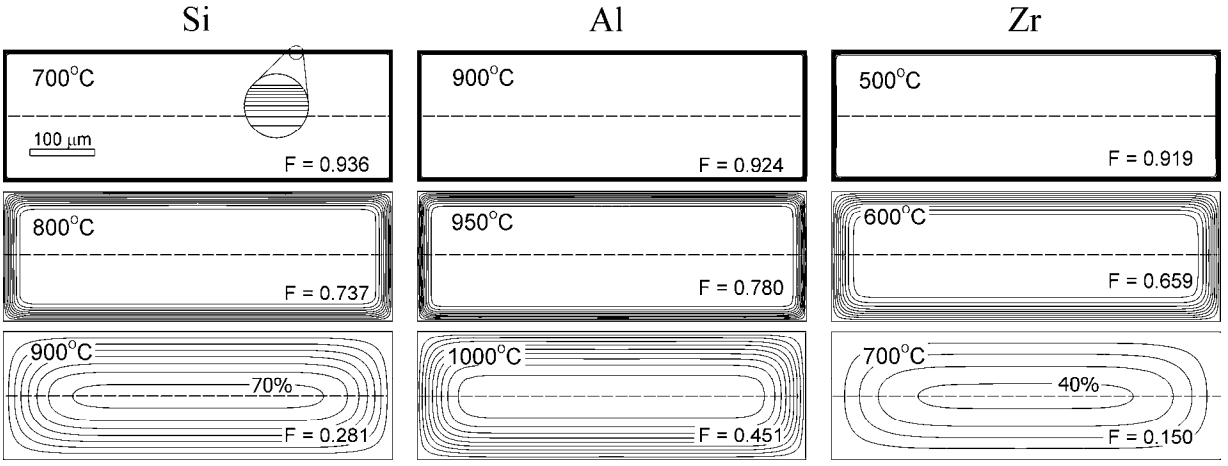

FIGURE 10. Results of diffusion calculations for a cylindrical model rutile crystal 200 μm in diameter and 600 μm long. The cylinder axis (dashed line) lies in the plane of the panels, which are contoured to show the diffusional response of Si, Al, and Zr at the temperatures indicated for a holding time of 10 million years. Contours represent a percent retention of the original element concentration at a given axial and radial location within the crystal. The contour interval is 10%; the innermost contour represents 90% retention except where indicated otherwise. F is the fraction of the element retained in the bulk crystal. The three temperatures modeled for each element were chosen to show the transition from essentially closed-system behavior (F > 0.9; top row) to severely compromised elemental concentrations (bottom row). See text for details.

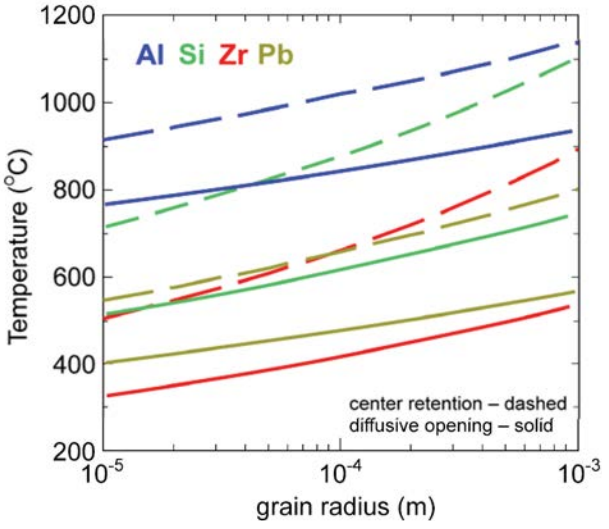

FIGURE 11. Conditions for diffusive "opening" (defined as loss of 1% of the diffusant) and center retention (equivalent to preservation of initial composition at grain center, but 50% loss of diffusant) for Al, Pb, Si, and Zr in rutile in the case of linear heating. Calculations are performed using Equation 1, a linear heating rate of 10 °C/Ma, the appropriate values of the constant χ_h for each criterion, and the diffusion parameters plotted in Figure 5. These calculations again illustrate the relative robustness of Al chemical signatures in rutile. (Color online.)

rutile, using the diffusion parameters of Cherniak et al. (2007a) and Cherniak (2000), respectively. This provides additional illustration of the comparatively high retentivity for Al chemical signatures in rutile; for example, Al would require heating to temperatures in excess of 840 °C to induce a 1% change in Al composition in 100 μm radius rutile grains, while comparable changes in Zr and Pb compositions would result when reaching temperatures of only ~420 and ~480 °C, respectively.

IMPLICATIONS

This study has shown that both Al and Si are among the slowest-diffusing species measured in rutile to date. With these slow diffusivities, the recently developed Al-in-rutile crystallization geothermobarometer (Hoff and Watson 2018) will be a robust indicator of past temperature and pressure conditions, more resistant to diffusional alteration than the Zr-in-rutile crystallization thermometer. In addition, should a Si-in-rutile thermometer become more fully developed, Si concentrations in rutile will likewise provide a crystallization thermometer resistant to alteration by diffusion.

ACKNOWLEDGMENTS AND FUNDING

This work was supported by NSF grant no. 1551381 to E.B.W. We thank Christopher Hoff for helpful discussions about Al and Si uptake in rutile. Constructive comments by reviewers Ralf Dohmen and Elias Bloch and Associate Editor Antonio Acosta-Vigil helped in improving the final version of the manuscript.

REFERENCES CITED

Akse, J.R., and Whitehurst, H.B. (1978) Diffusion of titanium in slightly reduced rutile. Journal of Physics and Chemistry of Solids, 39, 457–465.
Bak, T., Nowotny, J., Rekas, M., and Sorrell, C. (2003) Defect chemistry and semiconducting properties of titanium dioxide. Journal of Physics and Chemistry of Solids, 64, 1057–1067.
Bak, T., Bogdanoff, P., Fiechter, S., and Nowotny, J. (2012) Defect engineering of titanium dioxide: full defect disorder. Advances in Applied Ceramics, 111, 62–71.
Béjina, F., and Jaoul, O. (1996) Silicon self-diffusion in quartz and diopside measured by nuclear micro-analysis methods. Physics of Earth and Planetary Interiors, 97, 145–162.
——— (1997) Silicon diffusion in silicate minerals. Earth and Planetary Science Letters, 153, 229–238.
Boisvert, G., Lewis, L.J., and Yelon, A. (1995) Many-body nature of the Meyer-Neldel compensation law for diffusion. Physical Review Letters, 75, 469–472.
Brenan, J.M., Shaw, H.F., Phinney, D.L., and Ryerson, F.J. (1994) Rutile-aqueous fluid partitioning of Nb, Ta, Hf, Zr, U and Th; implications for high field strength element depletions in island-arc basalts. Earth and Planetary Science Letters, 128, 327–339.
Cherniak, D.J. (1993) Lead diffusion in titanite and preliminary results on the effects of radiation damage on Pb transport. Chemical Geology, 110, 177–194.
——— (1995) Diffusion of Pb in plagioclase and K-feldspar measured by Rutherford Backscattering spectroscopy and resonant nuclear reaction analysis. Contributions to Mineralogy and Petrology, 120, 358–371.

——— (2000) Pb diffusion in rutile. Contributions to Mineralogy and Petrology, 139, 198–207.
——— (2003) Silicon self-diffusion in single crystal natural quartz and feldspar. Earth Earth and Planetary Science Letters, 214, 655–668.
——— (2006) Zr diffusion in titanite. Contributions to Mineralogy and Petrology, 152, 639–647.
——— (2008) Si diffusion in zircon. Physics and Chemistry of Minerals, 35, 179–187.
Cherniak, D.J., and Watson, E.B. (1992) A study of strontium diffusion in K-feldspar, Na-K feldspar and anorthite using Rutherford Backscattering Spectroscopy. Earth and Planetary Science Letters, 411–425.
——— (2007) Ti diffusion in zircon. Chemical Geology, 242, 473–486.
Cherniak, D.J. Manchester, J., and Watson, E.B. (2007a) Zr and Hf diffusion in rutile. Earth and Planetary Science Letters, 261, 267–279.
Cherniak, D.J., Watson, E.B., and Wark, D.A. (2007b) Ti diffusion in quartz. Chemical Geology, 236, 65–74.
Corfu, F., and Andrews, A.J. (1986) A U-Pb age for mineralized Nipissing Diabase, Gowganda, Ontario. Canadian Journal of Earth Sciences, 23, 107–109.
Corfu, F., and Muir, T.L. (1989) The Hemlo-Heron Bay greenstone belt and Hemlo Au-Mo deposit, Superior Province, Ontario, Canada; 2, Timing of metamorphism, alteration and Au mineralization from titanite, rutile, and monazite U-Pb geochronology. Chemical Geology—Isotope Geoscience, 79, 201–223.
Crank, J. (1975) The Mathematics of Diffusion, 2nd ed., 414 pp. Oxford.
Cruz-Uribe, A.M., Feineman, M.D., Zack, T., and Jacob, D.E. (2018) Assessing trace element (dis)equilibrium and the application of single element thermometers in metamorphic rocks. Lithos, 314–315, 1–15.
Davis, W.J. (1997) U-Pb zircon and rutile ages from granulite xenoliths in the Slave Province; evidence for mafic magmatism in the lower crust coincident with Proterozoic dike swarms. Geology, 25, 343–346.
Deer, W.A., Howie, R.A., and Zussman, J. (1992) An Introduction to the Rock-forming Minerals. Longman Scientific Technical.
Degeling, H.S. (2003) Zr equilibria in metamorphic rocks. Unpublished Ph.D. thesis, Australian National University, 231 pp.
Demiryont, H. (1985) Optical properties of SiO_2-TiO_2 composite films. Applied Optics, 24, 2647–2650.
Dieckmann, R., Mason, T.O., Hodge, J.D., and Schmalzried, H. (1978) Defects and cation diffusion in magnetite (III.) Tracer diffusion of foreign tracer cations as a function of temperature and oxygen potential. Berichte der Bunsengesellschaft für Physikalische Chemie, 82, 778–783.
Dodson, M.H. (1973) Closure temperature in cooling geochronological and petrological systems. Contributions to Mineralogy and Petrology, 40, 259–274.
Dohmen, R., Chakraborty, S., and Becker, H.-W. (2002) Si and O diffusion in olivine and implications for characterizing plastic flow in the mantle. Geophysical Research Letters, 29, 26-1–26-4.
Dohmen, R., Marschall, H.R., Ludwig, T., and Polednia, J. (2018) Diffusion of Zr, Hf, Nb and Ta in rutile: effects of temperature, oxygen fugacity, and doping level, and relation to rutile point defect chemistry. Physics and Chemistry of Minerals. https://doi.org/10.1007/s00269-018-1005-7.
Escudero, A., and Langenhorst, F. (2012) Incorporation of Si into TiO_2 phases at high pressure. American Mineralogist, 97, 524–531.
Escudero, A., Langenhorst, F., and Müller, W.F. (2012) Aluminum solubility in TiO_2 rutile at high pressure and experimental evidence for a $CaCl_2$-structured polymorph. American Mineralogist, 97, 1075–1082.
Ewing, T.A., and Müntener, O. (2018) The mantle source of island arc magmatism during early subduction: Evidence from Hf isotopes in rutile from the Jijal Complex (Kohistan arc, Pakistan). Lithos, 308-309, 262–277.
Ewing, T.A., Hermann, J., and Rubatto, D. (2013) The robustness of the Zr-in-rutile and Ti-in-zircon thermometers during high-temperature metamorphism (Ivrea-Verbano Zone, northern Italy). Contributions to Mineralogy and Petrology, 165, 757–779.
Ferry, J.M., and Watson, E.B. (2007) New thermodynamic models and revised calibrations for the Ti-in-zircon and Zr-in-rutile thermometers. Contributions to Mineralogy and Petrology, 154, 429–437.
Fielitz, P., Borchardt, G., Schmücker, M., and Schneider, H. (2006) Al-26 diffusion measurement in 2/1-mullite by means of Secondary Ion Mass Spectrometry. Solid State Ionics, 177, 493–496.
Foley, S.F., Barth, M.G., and Jenner, G.A. (2000) Rutile/melt partition coefficients for trace elements and an assessment of the influence of rutile on the trace element characteristics of subduction zone magmas. Geochimica et Cosmochimica Acta, 64, 933–938.
Gaetani, G.A., Asimow, P.D., and Stolper, E.M. (2008) A model for rutile saturation in silicate melts with application to eclogite partial melting in subduction zones and mantle plumes. Earth and Planetary Science Letters, 272, 720–729.
Gesenhues, U. (1997) Doping of TiO_2 pigments by Al^{3+}. Solid State Ionics, Diffusion & Reactions, 101-103, 1171–1180.
Gesenhues, U., and Rentschler, T. (1999) Crystal growth and defect structure of Al^{3+}-doped rutile. Journal of Solid State Chemistry, 143, 210–218.
Golden, E.M., Giles, N.C., Shan Yang, and Halliburton, L.E. (2015) Interstitial silicon ions in rutile TiO_2 crystals. Physical Review B, 91, 134110.
Gonzalez-Elipe, A.R., Gracia, F., Yubero, F., Holgado, J.P., Espinos, J.P., and Girardeau, T. (2006) SiO_2/TiO_2 thin films with variable refractive index prepared by ion beam induced and plasma enhanced chemical vapor deposition. Thin Solid Films, 500, 19–26.
Guo, S., Tang, P., Su, B., Chen, Y., Ye, K., Zhang, L., Gao, Y., Liu, J., and Yang, Y. (2017) Unusual replacement of Fe-Ti oxides by rutile during retrogression in amphibolite-hosted veins (Dabie UHP Terrane); a mineralogical record of fluid-induced oxidation processes in exhumed UHP slabs. American Mineralogist, 102, 2268–2283.
Hatta, K., Higuchi, M., Takahashi, J., and Kodaira, K. (1996) Floating zone growth and characterization of aluminum-doped rutile single crystals. Journal of Crystal Growth, 163, 279–284.
Hayden, L.A., Watson, E.B., and Wark, D.A. (2008) A thermobarometer for sphene (titanite). Contributions to Mineralogy and Petrology, 155, 529–540.
Hoff, C.M., and Watson, E.B. (2018) Aluminum in rutile as a recorder of temperature and pressure. V.M. Goldschmidt Conference.
Hoshino, K., Peterson, N.L., and Wiley, C.L. (1985) Diffusion and point defects in TiO_{2-x}. Journal of Physics and Chemistry of Solids, 46, 1397–1411.
Islam, M.M., Bredow, T., and Gerson, A. (2007) Electronic properties of oxygen-deficient and aluminum-doped rutile TiO_2 from first principles. Physical Review B, 76, 045217.
Jaoul, O., Poumellec, M., Froidevaux, C., and Havette, A. (1981) Silicon diffusion in forsterite: A new constraint for understanding mantle deformation. In Stacey, F.D., Paterson, M.S., Nicholas, A., Eds., Anelasticity in the Earth, pp. 95–100. American Geophysical Union.
Jones, A.G. (2014) Compensation of the Meyer-Neldel Compensation Law for H diffusion in minerals. Geochemistry, Geophysics, Geosystems, 15, doi:10.1002/2014GC005261.
Karvinen, S. (2003) The effects of trace elements on the crystal properties of TiO_2. Solid State Science, 5, 811–819.
Kohn, M.J., Penniston-Dorland, S.C., and Ferreira, J.C.S. (2016) Implications of near-rim compositional zoning in rutile for geothermometry, geospeedometry, and trace element equilibration. Contributions to Mineralogy and Petrology, 171, 78.
Le Gall, M., Lesage, B., and Bernardini, J. (1994) Self-diffusion in Al_2O_3. I. Aluminum diffusion in single crystals. Philosophical Magazine, 70, 761–773.
Liu, L., Xiao, Y., Aulbach, S., Li, D., and Hou, Z. (2014) Vanadium and niobium behavior in rutile as a function of oxygen fugacity: evidence from natural samples. Contributions to Mineralogy and Petrology, 167, 1026.
Marschall, H.R., Dohmen, R., and Ludwig, T. (2013) Diffusion-induced fractionation of niobium and tantalum during continental crust formation. Earth and Planetary Science Letters, 375, 361–371.
Marucco, J.-F., Gautron, J., and Lemasson, P. (1981) Thermogravimetric and electrical study of nonstoichiometric titanium dioxide TiO_{2-x} between 800 and 1100 °C. Journal of Physics and Chemistry of Solids, 42, 363–367.
Mezger, K., Rawnsley, C.M., Bohlen, S.R., and Hanson, G.N. (1991) U-Pb garnet, sphene, monazite, and rutile ages; implications for the duration of high-grade metamorphism and cooling histories, Adirondack Mts., New York. Journal of Geology, 99, 415–428.
Mezger, K., Hanson, G.N., and Bohlen, S.R. (1989) High-precision U-Pb ages of metamorphic rutile; application to the cooling history of high-grade terranes. Earth and Planetary Science Letters, 96, 106–118.
Mitchell, R.J., and Harley, S.L. (2017) Zr-in-rutile resetting in aluminosilicate bearing ultra-high temperature granulites: Refining the record of cooling and hydration in the Napier Complex, Antarctica. Lithos, 272–273, 128–146.
Moore, D.K., Cherniak, D.J., and Watson, E.B. (1998) Oxygen diffusion in rutile from 750 to 1000 °C and 0.1 to 1000 MPa. American Mineralogist, 83, 700–711.
Morton, A.C., and Hallsworth, C.R. (1999) Processes controlling the composition of heavy mineral assemblages in sandstones. Sedimentary Geology, 124, 3–30.
Mosenfelder, J.D., Kim, N., and Stebbins, J.F. (2010) Silicon coordination in rutile and TiO_2-II at ambient and high pressures. American Mineralogist, 95, 968–973.
Nakayama, T., and Sasaki, T. (1963) The diffusion of barium in a rutile single crystal. Bulletin of the Chemical Society of Japan, 36, 569–574.
Nowotny, M.K., Bak, T., and Nowotny, J. (2006a) Electrical properties and defect chemistry of TiO_2 single crystal. III. Equilibrium kinetics and chemical diffusion. Journal of Physical Chemistry B, 110, 16292–16301.
——— (2006b) Electrical properties and defect chemistry of TiO_2 single crystal. IV. Prolonged oxidation kinetics and chemical diffusion. Journal of Physical Chemistry, B, 110, 16302–16308.
Paladino, A.E., and Kingery, W.D. (1962) Aluminum ion diffusion in aluminum oxide. Journal of Chemical Physics, 37, 957–962.
Pape, J., Mezger, K., and Robyr, M. (2016) A systematic evaluation of the Zr-in-rutile thermometer in ultra-high temperature (UHT) rocks. Contributions to Mineralogy and Petrology, 171, 44.
Ren, Y., Fei, Y., Yang, J., and Bai, W. (2009) SiO_2 solubility in rutile at high temperature and high pressure. Journal of Earth Sciences, 20, 274–283.
Ryerson, F.J., and Watson, E.B. (1987) Rutile saturation in magmas; implications

for Ti-Nb-Ta depletion in island-arc basalts. Earth and Planetary Science Letters, 86, 225–239.
Sakaguchi, I., Yurimoto, H., and Sueno, S. (1992) Impurities dislocation diffusion in single crystal MgO. Materials Science and Engineering, B 13, LI–L4.
Sasaki, J., Peterson, N.L., and Hoshino, K. (1985) Tracer impurity diffusion in single-crystal rutile (TiO_{2-x}). Journal of Physics and Chemistry of Solids, 46, 1267–1283.
Schandl, E.S., Davis, D.W., and Krogh, T.E. (1990) Are the alteration halos of massive sulfide deposits syngenetic? Evidence from U-Pb dating of hydrothermal rutile at the Kidd volcanic center, Abitibi Subprovince, Canada. Geology, 18, 505–508.
Slepetys, R.A., and Vaughan, P.A. (1969) Solid solution of aluminum oxide in rutile titanium oxide. Journal of Physical Chemistry, 73, 2157–2162.
Smye, A.J., and Stockli, D.F. (2014) Rutile U–Pb age depth profiling: A continuous record of lithospheric thermal evolution. Earth and Planetary Science Letters, 408, 171–182.
Stalder, R., Foley, S.F., Brey, G.P., and Horn, I. (1998) Mineral-aqueous fluid partitioning of trace elements at 900–1200 °C and 3.0–5.7 GPa; new experimental data for garnet, clinopyroxene, and rutile, and implications for mantle metasomatism. Geochimica et Cosmochimica Acta, 62, 1781–1801.
Stebbins, J.F. (2007) Aluminum substitution in rutile titanium dioxide: New constraints from high-resolution ^{27}Al NMR. Chemistry of Materials, 19, 1862–1869.
Tailby, N.D., Cherniak, D.J., and Watson, E.B. (2018) Al diffusion in quartz. American Mineralogist, 103, 839–847.
Taylor-Jones, K., and Powell, R. (2015) Interpreting zirconium-in-rutile thermometric results. Journal of Metamorphic Geology, 33, 115–122.
Thomas, J.B., Watson, E.B., Spear, F.S., Shemella, P.T., Nayak, S.K., and Lanzirotti, A. (2010) TitaniQ under pressure: the effect of pressure and temperature on the solubility of Ti in quartz. Contributions to Mineralogy and Petrology, 160, 743–759.
Tomkins, H.S., Powell, R., and Ellis, D.J. (2007) The pressure dependence of the zirconium-in-rutile thermometer. Journal of Metamorphic Geology, 25, 703–713.
Tual, L., Möller, C., and Whitehouse, M.J. (2018) Tracking the prograde P–T path of Precambrian eclogite using Ti-in quartz and Zr-in-rutile geothermobarometry. Contributions to Mineralogy and Petrology, 173, 56.
Van Orman, J.A., Li, C., and Crispin, K.L. (2009) Aluminum diffusion and Al-vacancy association in periclase. Physics of Earth and Planetary Interiors, 172, 34–42.
Vlassopoulos, D., Rossman, G.R., and Haggerty, S.E. (1993) Coupled substitution of H and minor elements in rutile and the implications of high OH contents in Nb- and Cr-rich rutile from the upper mantle. American Mineralogist, 78, 1181–1191.
Wark, D.A., and Watson, E.B. (2006) TitaniQ: A titanium-in-quartz geothermometer. Contributions to Mineralogy and Petrology, 152, 743–754.
Watson, E.B., and Cherniak, D.J. (2013) Simple equations for diffusion in response to heating. Chemical Geology, 335, 93–104.
Watson, E.B., and Harrison, T.M. (2005) Zircon thermometer reveals minimum melting conditions on earliest Earth. Science, 308, 841–844.
Watson, E.B., Wark, D.A., and Thomas, J.B. (2006) Crystallization thermometers for zircon and rutile. Contributions to Mineralogy and Petrology, 151, 413–433.
Watson, E.B., Wanser, K.H., and Farley, K.A. (2010) Anisotropic diffusion in a finite cylinder, with geochemical applications. Geochimica et Cosmochimica Acta, 74, 614–633.
Wong, L., Davis, D.W., Krogh, T.E., and Robert, F. (1991) U-Pb zircon and rutile chronology of Archean greenstone formation and gold mineralisation in the Val d'Or region, Quebec. Earth and Planetary Science Letters, 104, 325–336.
Yamazaki, D., Kato, T., Yurimoto, H., Ohtani, E., and Toriumi, M. (2000) Silicon self-diffusion in $MgSiO_3$ perovskite at 25 GPa. Physics of Earth and Planetary Interiors, 119, 299–309.
Zack, T., Kronz, A., Foley, S.F., and Rivers, T. (2002) Trace element abundances in rutiles from eclogites and associated garnet mica schists. Chemical Geology, 184, 97–122.
Zack, T., von Eynatten, H., and Kronz, A. (2004a) Rutile geochemistry and its potential use in quantitative provenance studies. Sedimentary Geology, 171, 37–58.
Zack, T., Moraes, R., and Kronz, A. (2004b) Temperature dependence of Zr in rutile: empirical calibration of a rutile thermometer. Contributions to Mineralogy and Petrology, 148, 471–488.
Zener, C. (1952) Theory of diffusion. In W. Shockley, J.H. Hollomon, R. Maurer, and F. Seitz, Eds., Imperfections in Nearly Perfect Crystals, pp. 289–314. Wiley.
Zhu, L., Ackland, G., Hu, Q.-M., Zhou, J., and Sun, Z. (2017) Origin of the abnormal diffusion of transition metal atoms in rutile. Physical Review B, 95, 245201.
Zhukova, I., O'Neill, H., and Campbell, I.H. (2017) A subsidiary fast-diffusing substitution mechanism of Al in forsterite investigated using diffusion experiments under controlled thermodynamic conditions. Contributions to Mineralogy and Petrology, 172, 53.
Ziegler, J.F., and Biersack, J.P. (2006) The stopping and range of ions in matter. Computer code SRIM 2006, http://www.srim.org.

Manuscript received March 4, 2019
Manuscript accepted July 26, 2019
Manuscript handled by Antonio Acosta-Vigil